This document is the Accepted Manuscript version of a Published Work that appeared in final form in
Industrial & Engineering Chemistry Research, copyright © American Chemical Society after peer review and technical editing by the publisher.
To access the final edited and published work see https://doi.org/10.1021/acs.iecr.9b00951

The Role of Mineral Nutrients in Plant-mediated Synthesis of 3D Porous $LaCoO_3$

*Kuncan Wang,[a] Junjie Huang,[a] Wen Li,[b] Jiale Huang,[a] Daohua Sun,[a] Xuebin Ke *[c] and Qingbiao Li *[a]*

[a] Department of Chemical and Biochemical Engineering, College of Chemistry and Chemical Engineering, National Laboratory for Green Chemical Productions of Alcohols, Ethers and Esters, Key Lab for Chemical Biology of Fujian Province, Xiamen University, Xiamen 361005, P. R. China.

[b] Department of Ecological Engineering for Environmental Sustainability, College of the Environment & Ecology, Xiamen University, Xiamen 361102, P. R. China.

[c] School of Engineering and Computer Science, University of Hull, HU6 7RX, United Kingdom.

KEYWORDS. Biosynthesis; Plant extract; Mineral nutrients; Perovskite $LaCoO_3$; Benzene oxidation

ABSTRACT. With the assistance of *Cacumen Platycladi* extract the facile synthesis of 3D porous $LaCoO_3$ perovskite is reported at a lower calcination temperature of 500 °C as compared with the traditional citric acid method. The formation mechanism is carefully studied by investigating the different roles of organic and inorganic components in several plant extracts. Two key factors to

create the porous structure of $LaCoO_3$ are identified involving in organic acid as complexing agent and nitrates for combustion-aid agents. The results indicate that organic components in the plant extract (mainly phenolic acids) function as the similar complex species of citric acid, while the mineral nutrients (Na^+, K^+, Ca^{2+} and Mg^{2+}) together with NO_3^- serve as combustion-aid agents even with trace amounts. Moreover, the biosynthesized $LaCoO_3$ in a low crystallization temperature has a high surface area of 32.5 m^2 g^{-1} and exhibits excellent catalytic performance for benzene oxidation. Six plant extracts demonstrate the similar functions for this biosynthesis. Benzene of 1000 ppm can achieve a stable conversion above 90% in a continuous run for 80 hours. It can be attributed to the bio-$LaCoO_3$ with more electrophilic adsorption of oxygen species and 3D porous structure.

Introduction

Biosynthesis is an eco-friendly approach to fabricating advanced materials, which shows the unparalleled advantages over other physical or chemical methods.[1-4] Plant extracts are readily available and have been employed to synthesize various nanoparticles (NPs).[5-8] Many studies have shown that organic ingredients in plant extract serve as reducing, chelating, capping, stabilizing agents as well as combustion fuels in the formation of metal NPs (MNPs) and metal oxide NPs (MONPs).[9-13] Karnan et al.[14] described the synthesis of ZnO NPs by using rambutan (*Nephelium lappaceum L.*) peel extract. And they demonstrated that phenolic components (one of biomolecules in extract) functioned as ligation agent. At the pH of 5-7, the aromatic hydroxyl groups of polyphenolic ellagic acid adhered to Zn^{2+} to form a stable zinc-ellagate complex system. After calcination, the uniform ZnO NPs were formed without significant agglomeration.

Mineral nutrients, such as Na^+, K^+, Ca^{2+}, Mg^{2+}, are nutrients for most of plant and exist in natural leaves at related low concentrations. Although the plausible mechanisms of plant-mediated synthesis of MONPs were proposed,[13] the role of these inorganic ingredients remains unknown. Actually, some reports have proved the existence of K^+,[15] Na^+,[16] Ca^{2+} [16] or other inorganic ingredients [17] but without further explorations. It is worth noting that alkali metal salts are often used as additives and play a special role in materials synthesis. In the solution combustion synthesis (SCS) route, a significant amount of NaCl or KCl (salt: metal = 0.5-2) were added to the precursor solution to limit the agglomeration and growth of the NPs, that is the so-called salt-assisted SCS.[18, 19] A similar case is that the introduction of NaF (Na: Ni = 0.5-1.5) into the SCS resulted in better particle dispersion and a drastic increase in specific surface area, compared with the conventional SCS.[20] In addition, sodium carboxymethylcellulose (Na: total metal = 2) as additive play a dual role (fuel and protecting agent) for the $BiVO_4$ synthesis.[21] Inspired by this, we wonder if the cations components of plant extracts, such as Na^+, K^+, Ca^{2+}, Mg^{2+}, play a significant role in plant-mediated synthesis even with trace amounts.

Perovskite-type oxides (PTOs) have been regarded as the promising substitutes for noble metals in the catalytic application.[22-24] $LaCoO_3$ has a high catalytic activity for oxidation reactions particularly. But the crystallization of $LaCoO_3$ often requires a high temperature (above 700 °C), which is hard to achieve porous texture (typically with a surface area less than 10 $m^2 g^{-1}$).[25,26] Many strategies[23] have been developed to improve textural properties of PTOs such as milling,[27] nanocasting or templating approaches,[28] solution-mediated processes (solvothermal and hydroxyacid complexation)[23] and microwave-assisted method.[29] A high surface area can be achieved (34-105 $m^2 g^{-1}$) through reducing crystallite size, forming porosity, suppressing grain

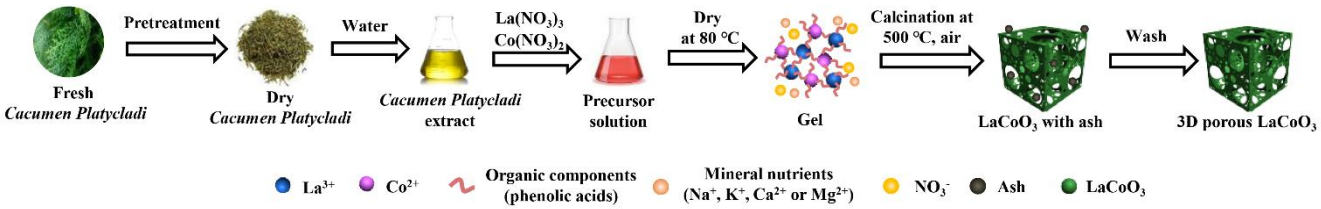

Scheme 1. Schematic illustration of the procedure to prepare bio-$LaCoO_3$.

growth or fast crystallization. Among these, simple and robust hydroxy acid complexion has received the attention due to its ease of scale up to obtain pure products with excellent textural properties.[23] Hence, the development of a facile and green synthesis strategy is paramount. Mayedwa et al.[30] reported the green synthesis of $ZnSnO_3$ nanoparticles by *Aspalathus Linearis* natural extracts recently, but the formation mechanism of PTOs was not mentioned, especially for the role of mineral nutrients.

In this work, for the first time, perovskite $LaCoO_3$ is biosynthesized by a sol-gel route with the aid of *Cacumen Platycladi* (CP) extract. More importantly, the special role of mineral nutrients (such as Na^+, K^+, Ca^{2+}, and Mg^{2+}) of plant extract is explored in the formation of a 3D porous structure at related low crystallization temperature. The obtained perovskite $LaCoO_3$ are also tested for catalytic oxidation of benzene.

Experimental Section

Materials

Cacumen Platycladi (CP) was purchased from Xiamen Jiuding Drugstore, China. *Oolong* tea was bought from the supermarket. *Cinnamomum camphora* leaf, *Nerium Indicum Mill.* leaf, *Rosa Chinensis* leaf, *Banyan* leaf, and *Grass* were collected from campus of Xiamen University. All leaves are washed three times with deionized water to remove foreign particles, and then dried at 80 °C. The pre-treated leaves were milled and screened by a 20-mesh sieve to get plant powders

for further experiments. Lanthanum nitrate, cobalt (II) nitrate, lanthanum acetate, cobalt (II) acetate, sodium nitrate, potassium nitrate, magnesium nitrate, calcium nitrate and citric acid were purchased from Aladdin Chemicals Co. Ltd, and were used as received.

Methods

Preparation of plant extract. For the *Cacumen Platycladi* extract and *Oolong* tea extract, 3.5 g plant powder was mixed with 100 mL deionized water. Thereafter, the mixture was shaken at a rotation rate of 170 rpm for 24 hours at 30 °C and finally filtrated, the filtrate concentration is 35 g L^{-1}. For other plant extracts, plant powders were carefully weighted and mixed with 100 mL deionized water. Then the mixture was boiled for 5 minutes with oil-bath and filtrated to get filtrate.

Biosynthesis of $LaCoO_3$. The bio-$LaCoO_3$ was prepared by a sol-gel process (Scheme 1). Specifically, lanthanum nitrate and cobalt nitrate (the molar ratio of La^{3+} to Co^{2+} ions is 1:1) were dissolved in 20 mL of CP extract under vigorous stirring at room temperature. After stirring for 1 hour, the solution was transferred to drying oven at 80 °C for 24 hours to form dry gels (denoted as bio-gel). Then the gels were calcined at 500 or 700 °C in air for 4 hours with a heating rate of 5 °C min^{-1} to obtain bio-$LaCoO_3$. Finally, the obtain catalysts were washed with 200 mL deionized water by filtrating and dry at 80 °C for 12 hours. The obtained samples were denoted as bio-500 and bio-700, respectively. The catalysts were tableted, crushed, and sieved to a size range of 40-80 mesh.

To examine the role of mineral nutrients, a CP extract concentration of 100 g L^{-1} was used to synthesize bio-500(A) and bio-500(M). For the bio-500(A), acetate ($La(CH_3COO)_3$ and

$Co(CH_3COO)_2$) were used as metallic precursor, while for the bio-500(M) mixed ($La(NO_3)_3$ and $Co(CH_3COO)_2$) precursors were used.

In addition, to explore the effect of CP extract concentration, a lower CP extract concentration of 20 g L^{-1} for bio-500(L) and a higher concentration of 45 g L^{-1} for bio-500(H) were adopted.

Catalyst evaluation. The catalytic activity for benzene oxidation was carried out in a continuous-flow quartz fixed-bed reactor (i.d. = 10 mm). 50 mg of the catalyst was used in each test. The gas mixture consisting of 1000 ppm benzene in air was fed into the reactor, and the total flow rate was kept at 33.4 mL min^{-1}, equivalent to a weight hourly space velocity (WHSV) of 40,000 mL g^{-1} h^{-1}. The benzene conversion was measured by determining the outlet concentration of benzene using an on-line GC equipped with a flame ionization detector (FID). The measurement of catalytic performance was made at steady state, typically after 30 minutes at each testing temperature

Catalyst characterization. X-ray diffraction (XRD) measurement was taken on an X'Pert Pro X-ray Diffractometer (PANalytical BV, The Netherlands) operated at a voltage of 35 kV and a current of 15 mA with a step size of 0.02°, using CuKa radiation. Samples morphology was observed by scanning electron microscopy (SEM, ZEISS SIGMA, Germany). Transmission electron microscopy (TEM) images were obtained on a Tecnai F30 microscope. N_2 physisorption was measured at 77 K on a BELSORP-mini II instrument. Before measurement, each sample was degassed at 250 °C for 3 hours. Functional groups of samples were investigated by Fourier transform infrared spectroscopy (FTIR, Nicolet 6700, USA). The thermo-gravimetric analysis (TGA, SDT Q600, USA) was performed for the thermal behaviour of samples. The representative samples were detected by XPS (Physical Electronics, USA) using a monochromatic Al Kα (1486.7 eV) as X-ray source in which the binding energy was calibrated with C 1s 284.8 eV.

Results and discussion

The role of CP extract in the formation of bio-$LaCoO_3$

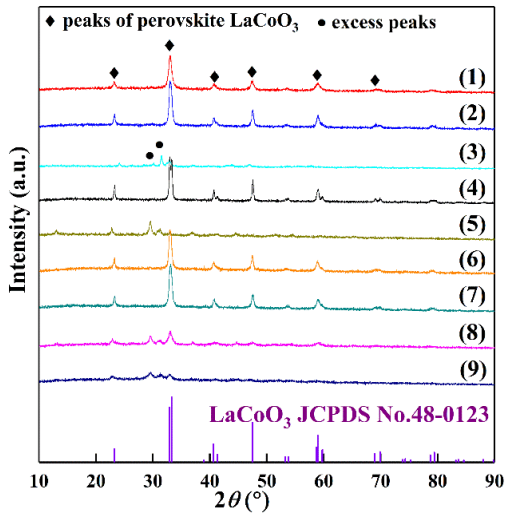

Figure 1. XRD patterns of (1) bio-500, (2) bio-700, (3) chem-500, (4) chem-700, (5) bio-500(A), (6) bio-500(M), (7) chem-500(S), (8) bio-500(L) and (9) bio-500(H).

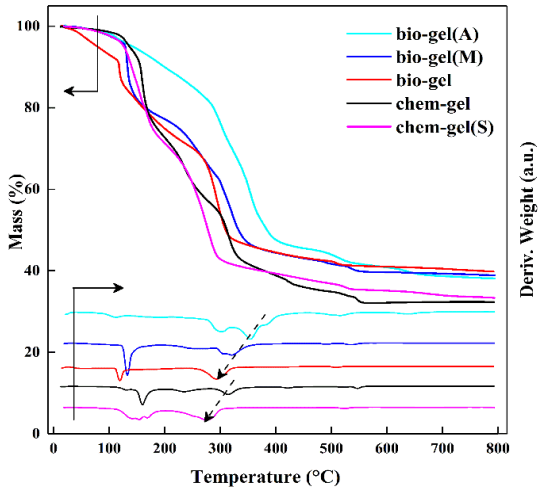

Figure 2. TG and DTG curves of different samples.

The XRD patterns show that the perovskite structure $LaCoO_3$ are obtained for the samples of bio-500 and bio-700 (Figure 1), which match well with the standard (JCPDS No. 48-0123).[31] Similar with previous studies,[26, 32] several excess diffraction peaks (2θ = 24-32°) for chem-500 (sample 3) are observed, which suggests a difficulty to obtain pure $LaCoO_3$ phase at a lower temperature through the conventional method. When the calcination temperature is raised to 700 °C (chem-700, sample 4), a pure perovskite phase of $LaCoO_3$ can be obtained. Hence, the biosynthesis of perovskite structure $LaCoO_3$ can be achieved at a low calcination temperature down to 500 °C. In addition, it got a mixed phase if the concentration of CP extract is lower (bio-500(L), sample 8) or higher (bio-500(H), sample 9). Therefore, a moderate concentration is a necessity to obtain pure perovskite structure of $LaCoO_3$ at 500 °C.

Inductively coupled mass spectrometry (ICP-MS, Agilent 7500CE) combined with concentric nebulizer is used to determine the concentration of mineral nutrients (Na^+, K^+, Ca^{2+}, and Mg^{2+}) in extracts. Table 1 shows the distribution of these mineral nutrients in six different types of leaf extracts. Even in the same leaf extract, the concentration of different ions is distinctly different. K^+ exhibits the greatest amount for most of plant extracts and the concentration of Na^+ is the lowest. To determine the role of mineral nutrients, chem-500(S) are synthesized by adding $NaNO_3$, KNO_3, $Ca(NO_3)_2$ and $Mg(NO_3)_2$. A pure phase of perovskite $LaCoO_3$ is obtained for chem-500(S) (Figure 1, sample 7). Thus, it can be concluded that the nitrates play a special role in the formation of $LaCoO_3$.

Further, bio-500(A) has no XRD diffraction peaks of $LaCoO_3$ and bio-500(M) turns to pure perovskite (Figure 1, sample 5 and sample 6). These two samples have different ions in gels before calcination (Table 2): the big difference lies in the existence of NO_3^- in the gel of bio-500(A). The introduction of NO_3^- into plant extract accounts for the low temperature crystallization of $LaCoO_3$. Accordingly, mineral nutrients (Na^+, K^+, Ca^{2+} and Mg^{2+}) in the plant extract together with NO_3^- lead to the crystallization of $LaCoO_3$ at a low temperature of 500 °C.

Table 1. Concentration (mg L^{-1}) of mineral nutrients in different leaf extracts (10 g leaf powder in 1 L deionized water).

Ions	*Cacumen Platycladi*	*Oolong* tea	*Cinnamomum camphora*	*Grass*	*Nerium Indicum Mill.*	*Rosa Chinensis*
Na^+	0.30	0.25	0.44	0.70	0.66	28.61
K^+	25.62	192.10	53.49	167.9	129.90	337.20
Ca^{2+}	18.42	6.48	59.58	12.68	12.48	16.51
Mg^{2+}	3.60	8.59	14.1	6.03	16.49	20.66

Table 2. Summary of Ions, the highest decomposition temperature and final crystal phase (product) for different gels.

samples	Na^+	K^+	Ca^{2+}	Mg^{2+}	CH_3COO^-	NO_3^-	decomposition temperature[a] (°C)	crystal phase[b]
bio-gel(A)	√	√	√	√	√	×	385	mixed phase
bio-gel(M)	√	√	√	√	√	√	320	pure phase
bio-gel	√	√	√	√	×	√	290	pure phase
chem-gel	×	×	×	×	×	√	315	mixed phase
chem-gel(S)	√	√	√	√	×	√	275	pure phase

Notes: √ existed; × not existed. [a] Determined from DTG curves (Figure 2), [b] Determined from XRD (Figure 1).

To reveal the role of mineral nutrients in plant extract, thermal analysis is conducted on the gels collected from the precursors of bio-500(A), bio-500(M), bio-500, chem-500 and chem-500(S) (denoted as bio-gel(A), bio-gel(M), bio-gel, chem-gel and chem-gel(S), respectively). As shown in Figure 2, several weight loss stages rather than an abrupt weight loss are observed between 100-500 °C, which is a characteristic of sol-gel synthesis route.[20] It can be seen from the DTA curves that the highest decomposition temperature (Table 2) gradually decreased from 385 °C (bio-gel(A)) to 320 °C (bio-gel(M)) and 290 °C (bio-gel) when nitrates are added. Without the mineral nutrients, the decomposition temperature of chem-gel maintains a high value of 315 °C compared to chem-gel(S) at 275 °C even with the existence of nitrates. Obviously, both mineral nutrients and nitrates are the key factors for the decrease of decomposition temperature, and therefore promoting the crystallization. We propose that the oxidants like $NaNO_3$ and KNO_3 can be formed locally while mineral nutrients (Na^+, K^+, Ca^{2+}, and Mg^{2+} in CP extract) mix with NO_3^-, which accelerate the intense decomposition of organic components.[18, 19] The released heat locally contributes significantly to the crystallization of perovskite $LaCoO_3$. From this point of view, mineral nutrients in CP extract together with NO_3^- function as combustion-aid agents.

Various organic components in plant extracts often act as complexing agents, which can bound with cations to stabilized the metal oxide NPs and prevent crystal over-growth.[11] Herein, organic components with carboxyl group in the plant extract are expected to be complexing agent for the

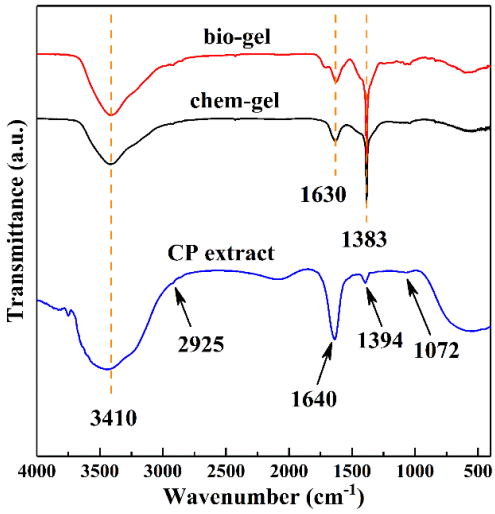

Figure 3. Infrared spectra (FT-IR) of different samples.

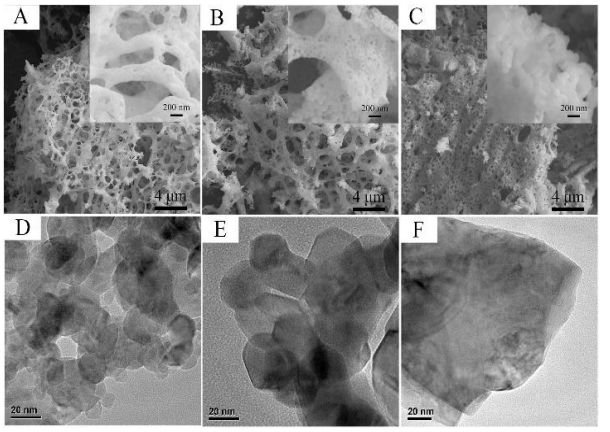

Figure 4. SEM images of: (A) bio-500, (B) bio-700, (C) chem-700. The insets are high magnification SEM images of corresponding samples. And TEM images of: (D) bio-500, (E) bio-700, (F) chem-700.

biosynthesis of $LaCoO_3$. To be verified, FT-IR spectra are used to identify the complexing agent of CP extract (Figure 3). The samples of CP extract, bio-gel and chem-gel show the same absorption band at 3410 cm^{-1} , which should be assigned to the O–H stretching vibrations of residual water.[33] The CP extract shows significant absorption bands at 2925, 1640, 1394 and 1072 cm^{-1}, which are associated with the stretch vibration of C–H in aromatic compound, C=O in conjugate carboxylic acid, O–H in the phenol group, C–O in phenolic acid, respectively.[33-36] These characteristic peaks suggest the existence of phenolic acids in CP extract, which contain a phenolic ring and an organic carboxylic acid function.[37] And the bio-gel and chem-gel show similar spectra with two sharp bands at 1630 and 1383 cm^{-1}, which are attributed to the symmetric and asymmetric vibration of COO^-, respectively. The frequency separation ($\Delta\nu$ = 247 cm^{-1}) between the asymmetric stretching $\nu_{asym}(COO^-)$ vibration and symmetric stretching $\nu_{sym}(COO^-)$ vibration suggests that acetate anions act as bridging bidentate ligands.[38] These results demonstrate that conjugated carboxyl groups in CP extract can chelate with cations (La^{3+} and Co^{2+}), promoting the formation of perovskite $LaCoO_3$.

Above all, the organic components (mainly phenolic acid) in plant extract act as the similar complex species of citric acid, while the mineral nutrients together with NO_3^- served as combustion-aid agents, both promote the formation of perovskite $LaCoO_3$ at a low temperature.

Morphology, textural and surface properties of bio-$LaCoO_3$

The morphology of representative samples is investigated by SEM and TEM. A 3D porous structure can be observed from the bio-500 and bio-700 samples (Figure 4A and 4B), while a bulk structure with much less holes is found in chem-700 (Figure 4C).[20] The results can be further confirmed by the high-magnification SEM images (the insets in Figure 4A, 4B and 4C) and very fine particles are observed for the bio-500 and bio-700 samples. The TEM image shows stacked nanoparticles with a diameter less than 20 nm for the bio-500 sample (Figure 4D) in consistent with the XRD results, which is determined by the Scherrer equation at 2θ of 23.23° and the average particle sizes is ca. 15.3 nm.[39] As for bio-700, a larger size of 20-30 nm is observed (Figure 4E) while the calculation from the XRD patterns is ca. 25 nm. In contrast, the bulk without holes and fine nanoparticles can be seen for the chem-700 sample (Figure 4F). The 3D porous structures originate from the liberation of organic components during the calcination, which is intensified by combustion-aid agents.[20] This is evidenced by similar morphology and structure for chem-500(S) without CP extracts (SEM and TEM images in Figure S1, Supporting Information). However, the lower CP extract concentration (bio-500(L)) results in the substantial agglomeration while a 3D porous structure can be maintained in higher CP extract concentration (bio-500(H)), shown in Figure S1 of Supporting Information. These indicate that the combustion aid of sufficient mineral nutrients is indispensable.

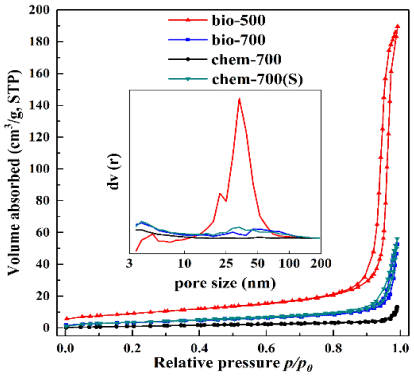

Figure 5. N_2 adsorption-desorption isotherms. The inset is the pore-size distributions.

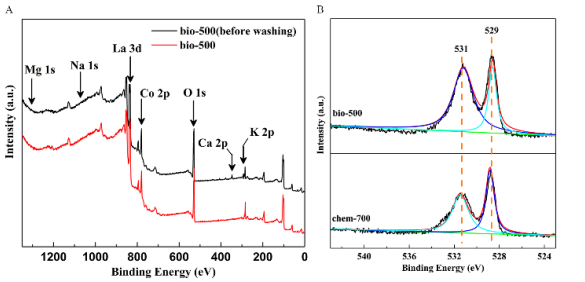

Figure 6. (A) XPS spectra of bio-500 (before washing) and bio-500; (B) O 1s XPS spectra of bio-500 and chem-700.

The nitrogen adsorption-desorption isotherms (Figure 5) show the hysteresis loops at P/P_0 = 0.8-0.9 corresponding to the gaps piled up by nanoparticles.[31, 40]. The textural properties are shown in Table 3. The surface area for chem-700 is 4.8 m^2 g^{-1}, which is typically less than 10 m^2 g^{-1} via the citric acid complex method.[32] The surface area increases for bio-700 sample while using CP extracts (12.9 m^2 g^{-1}) and a high surface area of 32.5 m^2 g^{-1} is achieved for the bio-500 sample, which may be originated from fine nanoparticles without aggregation at a lower calcination temperature. Moreover, the bio-500 sample show a porous structure ranging from 20 nm to 70 nm (Figure 5), which agrees well with the morphology observation. The surface area of chem-700(S) is 13.4 m^2 g^{-1} while adding mineral nutrients and nitrates, which significantly contribute to porous structure as well.

Table 3. Textural and surface properties of the representative samples.

Samples	BET surface area[a] (m^2 g^{-1})	Pore volume[b] (cm^3 g^{-1})	Average pore radius (nm)	Na[c]	K[c]	Ca[c]	Mg[c]	O_{ads}/O_{latt}[d]
bio-500bf	-	-	-	0.11	1.87	1.42	0.20	-
bio-500	32.5	0.289	35.5	*	*	0.30	*	2.43
bio-700	12.9	0.080	24.8	-	-	-	-	-
chem-700	4.8	0.020	16.2	-	-	-	-	1.0

Notes: bio-500bf represents a sample before washing; * means the components are not detectable by XPS. - No data. [a] Derived from nitrogen adsorption isotherms in the P/P_0 range of 0.05-0.35. [b] Determined from the data adsorbed at P/P_0 = 0.99. [c] Calculated based on the XPS spectra (Atomic %). [d] Calculated based on the XPS spectra.

XPS test is performed to examine the elemental composition difference on the surface (Figure 6A). Na, K, Ca and Mg components are detected for bio-500 (before washing), and the atomic

ratio of La: Na: K: Ca: Mg = 1: 0.01: 0.20: 0.02: 0.16. After the rinsing process, Na, K and Mg components disappear and only trace of Ca species remain (Table 3).

Electrophilic oxygen species (O_{ads}, e.g., O_2^-, O_2^{2-}, O^-.) play a vital role in the deep oxidation of benzene.[40] The O 1s spectra of bio-500 and chem-700 are shown in Figure 6B to investigate the surface oxygen species. Two distinct peaks are about 531 and 529 eV are assigned to electrophilic O_{ads}, and surface lattice oxygen (O_{latt}).[41] The O_{ads}/O_{latt} ratio of bio-500 (2.43) is higher than chem-700 (1.00), which indicates much higher deep oxidation ability (Table 3).

Possible mechanism

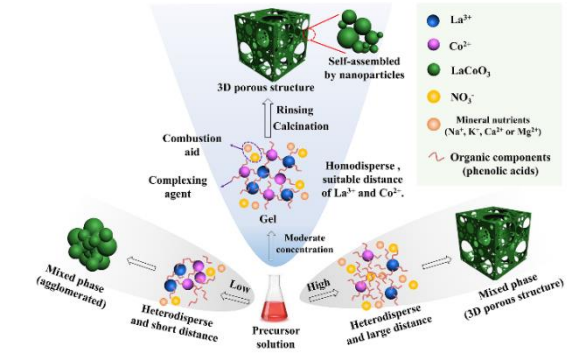

Scheme 2. Schematic illustrations for the formation of bio-$LaCoO_3$.

A possible mechanism for green synthesis of $LaCoO_3$ by CP extract is proposed (Scheme 2). Traditionally, $LaCoO_3$ often crystallize at a high temperature of above 700 °C.[23, 33, 42] In this work CP extract (containing organic components and mineral nutrients), NO_3^- (from metal precursor) and the dispersion of La^{3+} and Co^{2+} are key factors in the formation of pure-phase $LaCoO_3$ at a low temperature of 500 °C.

The precursor solution is obtained by mixing CP extract with $La(NO_3)_3$ and $Co(NO_3)_2$. At a moderate CP extract concentration, the organic components contained -COOH (phenolic acids) in CP extract function as complexing agent, which helps La^{3+} and Co^{2+} to form homogeneous gel

with excellent dispersion.[33, 36] More importantly, combustion-aid agents are formed while mineral nutrients (Na^+, K^+, Ca^{2+} and Mg^{2+}) mixed with NO_3^-, which can intensify the combustion of the organic components in CP extract during calcination. With the assistance of the combustion-aid agents, the locally intensive heat facilitates the uniform crystallization of $LaCoO_3$ and create a porous structure at relative low temperature.

At a low CP extract concentration, less amounts of organic components and mineral nutrients cannot create porous structure of $LaCoO_3$. At a high CP extract concentration, the high concentration complexing agents of organic components may suppress the crystallization of $LaCoO_3$ although a 3D porous structure can be formed at related low calcination temperatures.[33,36]

Given that plants are available extensively and have similar chemical compositions, six plant leaves including *Oolong* tea, *Cinnamomum camphora*, *Nerium Indicum Mill.*, *Rosa Chinensis*, *Banyan* and *Grass* are collected to biosynthesize $LaCoO_3$ at 500 °C. Perovskite $LaCoO_3$ with porous structure is obtained evidenced by XRD patterns and SEM images (Figures S2 and S3, Supporting Information), which suggests the extensive applicability of plant extracts for green synthesis of $LaCoO_3$.

Catalytic performances

The catalytic activity for benzene oxidation is determined by the indicator T_{90}, which is the temperature when the benzene conversion rate reaches 90%. The bio-500 (before washing) exhibits a low catalytic activity with T_{90} > 500 °C and the catalytic activity for bio-500 (after rinsing) is significantly enhanced with a T_{90} of 285 °C (Figure 7A), which can be ascribed to the removal of residual ash from mineral nutrients in CP extract (Table 3). Compared with the T_{90} of

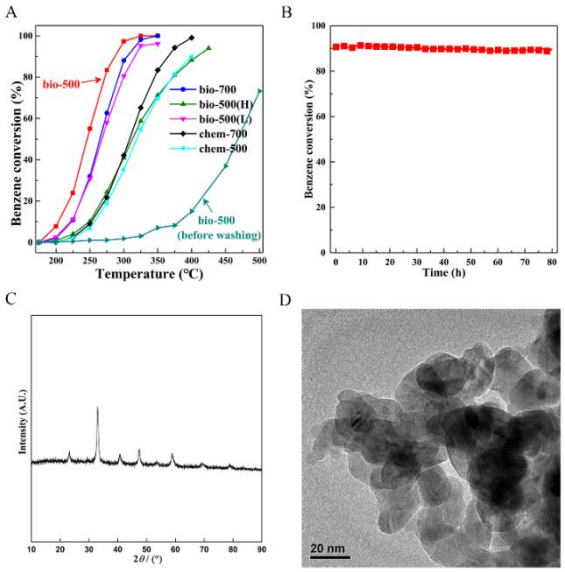

Figure 7. (A) Benzene conversion as a function of reaction temperature; (B) The time-on-stream data collected over bio-500 at 285 °C (C) XRD pattern and (D) TEM image of the spent bio-500 after activity evaluation of 80 h.

chem-700 (365 °C), T_{90} of bio-500 and bio-700 decrease about and 60-80°C. Hence, the biosynthesized $LaCoO_3$ exhibits much better catalytic performance than traditionally chemical synthesis, which should be attributed to its abundant electrophilic O_{ads} on the surface.

The samples of mixed phase, such as bio-500(L), bio-500(H) and chem-500, shows related low catalytic activity. But the catalytic performance of chem-500(S) is very close to bio-500 as they have little difference in crystal phase, morphologies, structural, textural and surface properties, (Figure S4, Supporting Information).

The stability of bio-500 is tested and shows no deactivation for continuous reaction of 80 hours. Furthermore, the XRD pattern and TEM image of the spent bio-500 shows no identifiable phase changes or obvious particle aggregation (Figure 7) As a result, the biosynthesized $LaCoO_3$ possesses a high thermal stability in catalytic oxidation of benzene.

Conclusions

In summary, a green method has been developed to synthesize 3D porous $LaCoO_3$ utilizing plant extracts at low-temperature calcination. The control experiments and TG analysis indicate that mineral nutrients (Na^+, K^+, Ca^{2+} and Mg^{2+}) act as combustion-aid agents while mixing with NO_3^-, which can significantly decrease the crystallization temperature of $LaCoO_3$ and promote the formation of a porous structure. To the best of our knowledge, this is a new understanding of plant-meditated synthesis as many previous studies focused on the role of organic components alone. This green method can be extended to the synthesis of 3D porous $LaCoO_3$ with other six plant extracts. More importantly, the biosynthesized $LaCoO_3$ has an excellent catalytic performance for benzene oxidation, for instance, to lower down the reaction temperature up to 80°C and stably run for 80 hours. This synthesis strategy can be extended to other materials manufacturing with scale-up capability embedded.

ASSOCIATED CONTENT

Supporting Information. Supporting Information are available for detailed materials characterization.

AUTHOR INFORMATION

Corresponding Author

* kelqb@xmu.edu.cn (Qingbiao Li); * x.ke@hull.ac.uk (Xuebin Ke).

ACKNOWLEDGMENT

This work was supported by the National Natural Science Foundation of China (No. 21536010 and No. 41673088). Prof. Guowu Zhan in Huaqiao University and Dr. Mingzhi Wang in Xiamen University are gratefully acknowledged for their helpful discussion.

REFERENCES

[1] G.T. Zan, Q.S. Wu, Biomimetic and bioinspired synthesis of nanomaterials/Nanostructures, Adv. Mater., 28 (2016) 2099-2147.

[2] J.L. Huang, L.Q. Lin, D.H. Sun, H.M. Chen, D.P. Yang, Q.B. Li, Bio-inspired synthesis of metal nanomaterials and applications, Chem. Soc. Rev., 44 (2015) 6330-6374.

[3] S.A. Dahoumane, M. Mechouet, K. Wijesekera, C.D.M. Filipe, C. Sicard, D.A. Bazylinski, C. Jeffryes, Algae-mediated biosynthesis of inorganic nanomaterials as a promising route in nanobiotechnology-a review, Green Chem., 19 (2017) 552-587.

[4] S. Kim, C.B. Park, Bio-Inspired synthesis of minerals for energy, environment, and medicinal applications, Adv. Funct. Mater., 23 (2013) 10-25.

[5] P.K. Rai, V. Kumar, S. Lee, N. Raza, K.-H. Kim, Y.S. Ok, D.C.W. Tsang, Nanoparticle-plant interaction: implications in energy, environment, and agriculture, Environ. Int., 119 (2018) 1-19.

[6] P. Basnet, T.I. Chanu, D. Samanta, S. Chatterjee, A review on bio-synthesized zinc oxide nanoparticles using plant extracts as reductants and stabilizing agents, J. Photochem. Photobiol. B-Biol., 183 (2018) 201-221.

[7] A.K. Shukla, S. Iravani, Metallic nanoparticles: green synthesis and spectroscopic characterization, Environ. Chem. Lett., 15 (2017) 223-231.

[8] S. Iravani, Green synthesis of metal nanoparticles using plants, Green Chem., 13 (2011) 2638-2650.

[9] G. Nabi, A. Qurat ul, N.R. Khalid, M.B. Tahir, M. Rafique, M. Rizwan, S. Hussain, T. Iqbal, A. Majid, A review on novel eco-friendly green approach to synthesis TiO_2 nanoparticles using different extracts, J. Inorg. Organomet. Polym. Mater., 28 (2018) 1552-1564.

[10] P. Vishnukumar, S. Vivekanandhan, M. Misra, A.K. Mohanty, Recent advances and emerging opportunities in phytochemical synthesis of ZnO nanostructures, Mater. Sci. Semicond. Process., 80 (2018) 143-161.

[11] S. Ahmed, Annu, S.A. Chaudhry, S. Ikram, A review on biogenic synthesis of ZnO nanoparticles using plant extracts and microbes: a prospect towards green chemistry, J. Photochem. Photobiol. B: Biol., 166 (2017) 272-284.

[12] J. Jeevanandam, Y.S. Chan, M.K. Danquah, Biosynthesis of metal and metal oxide nanoparticles, ChemBioEng Rev., 3 (2016) 55-67.

[13] S.A.O. Santos, R.J.B. Pinto, S.M. Rocha, P. Marques, C.P. Neto, A.J.D. Silvestre, C.S.R. Freire, Unveiling the chemistry behind the green synthesis of metal nanoparticles, ChemSusChem, 7 (2014) 2704-2711.

[14] T. Karnan, S.A.S. Selvakumar, Biosynthesis of ZnO nanoparticles using rambutan (Nephelium lappaceumL.) peel extract and their photocatalytic activity on methyl orange dye, J. Mol. Struct., 1125 (2016) 358-365.

[15] M. Khatami, H.Q. Alijani, H. Heli, I. Sharifi, Rectangular shaped zinc oxide nanoparticles: green synthesis by Stevia and its biomedical efficiency, Ceram. Int., 44 (2018) 15596-15602.

[16] B.T. Sone, E. Manikandan, A. Gurib-Fakim, M. Maaza, Sm_2O_3 nanoparticles green synthesis via Callistemon viminalis' extract, J. Alloys Compd., 650 (2015) 357-362.

[17] G. Nandhini, R. Suriyaprabha, W.M.S. Pauline, V. Rajendran, W.K. Aicher, O.K. Awitor, Influence of solvents on the changes in structure, purity, and in vitro characteristics of green-synthesized ZnO nanoparticles from Costus igneus, Appl. Nanosci., 8 (2018) 1353-1360.

[18] A. Varma, A.S. Mukasyan, A.S. Rogachev, K.V. Manukyan, Solution combustion synthesis of nanoscale materials, Chem. Rev., 116 (2016) 14493-14586.

[19] W.F. Chen, F.S. Li, J.Y. Yu, L.L. Liu, H.L. Gao, Rapid synthesis of mesoporous ceria-zirconia solid solutions via a novel salt-assisted combustion process, Mater. Res. Bull., 41 (2006) 2318-2324.

[20] W. Wen, J.-M. Wu, Eruption combustion synthesis of NiO/Ni nanocomposites with enhanced properties for dye-absorption and lithium Storage, ACS Appl. Mater. Interfaces, 3 (2011) 4112-4119.

[21] U.M. García Pérez, S. Sepúlveda-Guzmán, A. Martínez-de la Cruz, U. Ortiz Méndez, Photocatalytic activity of $BiVO_4$ nanospheres obtained by solution combustion synthesis using sodium carboxymethylcellulose, J. Mol. Catal. A: Chem., 335 (2011) 169-175.

[22] J. Hwang, R.R. Rao, L. Giordano, Y. Katayama, Y. Yu, Y. Shao-Horn, Perovskites in catalysis and electrocatalysis, Science, 358 (2017) 751-756.

[23] S.C.b. Royer, D. Duprez, F. Can, X. Courtois, C. Batiot-Dupeyrat, S. Laassiri, H. Alamdari, Perovskites as substitutes of noble metals for heterogeneous catalysis: dream or reality, Chem. Rev., 114 (2014) 10292-10368.

[24] J.J. Zhu, H.L. Li, L.Y. Zhong, P. Xiao, X.L. Xu, X.G. Yang, Z. Zhao, J.L. Li, Perovskite oxides: preparation, characterizations, and applications in heterogeneous catalysis, ACS Catal., 4 (2014) 2917-2940.

[25] H.Y. Zhu, P.F. Zhang, S. Dai, Recent advances of lanthanum-based perovskite oxides for catalysis, ACS Catal., 5 (2015) 6370-6385.

[26] E. Ghiasi, A. Malekzadeh, M. Ghiasi, Moderate concentration of citric acid for the formation of $LaMnO_3$ and $LaCoO_3$ nano-perovskites, J. Rare Earths, 31 (2013) 997-1002.

[27] S. Kaliaguine, V. Szabo, A. Van Neste, J.E. Gallot, M. Bassir, R. Muzychuk, Perovskite-type oxides synthesized by reactive grinding, in: R. Schulz (Ed.) Electrochemical and Chemical Reactivity of Amorphous and Nanocrystalline Materials, Trans Tech Publications Ltd, Stafa-Zurich, 2001, pp. 39-56.

[28] Y. Wang, J. Ren, Y. Wang, F. Zhang, X. Liu, Y. Guo, G. Lu, Nanocasted synthesis of mesoporous $LaCoO_3$ perovskite with extremely high surface area and excellent activity in methane combustion, J. Phys. Chem. C, 112 (2008) 15293-15298.

[29] I.S. Yakovleva, A.V. Kuznetsova, E.Y. Gerasimov, A.A. Pochtar, L.A. Isupova, Microwave synthesis of $LaBO_3$ (B = Co, Fe) perovskites using graphite and citric acid additions, Kinet. Catal., 55 (2014) 630-638.

[30] N. Mayedwa, N. Mongwaketsi, S. Khamlich, K. Kaviyarasu, N. Matinise, M. Maaza, Green synthesis of zin tin oxide ($ZnSnO_3$) nanoparticles using Aspalathus Linearis natural extracts: Structural, morphological, optical and electrochemistry study, Appl. Surf. Sci., 446 (2018) 250-257.

[31] Y. Luo, K. Wang, J. Zuo, Q. Qian, Y. Xu, X. Liu, H. Xue, Q. Chen, Selective corrosion of $LaCoO_3$ by NaOH: structural evolution and enhanced activity for benzene oxidation, Catal. Sci. Technol., 7 (2017) 496-501.

[32] H. Taguchi, S. Yamada, M. Nagao, Y. Ichikawa, K. Tabata, Surface characterization of $LaCoO_3$ synthesized using citric acid, Mater. Res. Bull., 37 (2002) 69-76.

[33] Z. Shao, G. Xiong, Y. Ren, Y. Cong, W. Yang, Low temperature synthesis of perovskite oxide using the adsorption properties of cellulose, J. Mater. Sci., 35 (2000) 5639-5644.

[34] K. Jeeva, M. Thiyagarajan, V. Elangovan, N. Geetha, P. Venkatachalam, Caesalpinia coriaria leaf extracts mediated biosynthesis of metallic silver nanoparticles and their antibacterial activity against clinically isolated pathogens, Ind. Crop. Prod., 52 (2014) 714-720.

[35] K. Jagajjanani Rao, S. Paria, Green synthesis of silver nanoparticles from aqueous Aegle marmelos leaf extract, Mater. Res. Bull., 48 (2013) 628-634.

[36] Z. Shao, G. Li, G. Xiong, W. Yang, Modified cellulose adsorption method for the synthesis of conducting perovskite powders for membrane application, Powder Technol., 122 (2002) 26-33.

[37] P. Dauthal, M. Mukhopadhyay, Noble metal nanoparticles: plant-mediated synthesis, mechanistic aspects of synthesis, and applications, Ind. Eng. Chem. Res., 55 (2016) 9557-9577.

[38] L. Predoana, B. Malic, M. Kosec, M. Carata, M. Caldararu, M. Zaharescu, Characterization of $LaCoO_3$ powders obtained by water-based sol-gel method with citric acid, J. Eur. Ceram. Soc., 27 (2007) 4407-4411.

[39] S. Farhadi, S. Sepahvand, Microwave-assisted solid-state decomposition of La $[Co(CN)_6]\cdot 5H_2O$ precursor: A simple and fast route for the synthesis $LaCoO_3$ nanoparticles, J. Alloys Compd., 489 (2010) 586-591.

[40] Y. Luo, K. Wang, J. Zuo, Q. Qian, Y. Xu, X. Liu, H. Xue, Q. Chen, Enhanced activity for total benzene oxidation over SBA-15 assisted electrospun $LaCoO_3$, Molecular Catalysis, 436 (2017) 259-266.

[41] Y.J. Feng, L. Li, S.F. Niu, Y. Qu, Q. Zhang, Y.S. Li, W.R. Zhao, H. Li, J.L. Shi, Controlled synthesis of highly active mesoporous Co_3O_4 polycrystals for low temperature CO oxidation, Appl. Catal., B, 111 (2012) 461-466.

[42] M.S.G. Baythoun, F.R. Sale, Production of strontium-substituted lanthanum manganite perovskite powder by the amorphous citrate process, J. Mater. Sci., 17 (1982) 2757-2769.

SYNOPSIS (Word Style “SN_Synopsis_TOC”). If you are submitting your paper to a journal that requires a synopsis, see the journal’s Instructions for Authors for details.

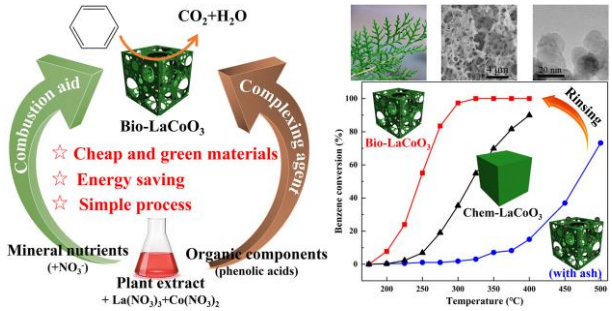

Mineral nutrients in plant extract served as combustion-aid agent result in lower temperature formation of 3D porous $LaCoO_3$.